Published in final edited form as:

Mol Cancer Ther. 2016 May ; 15(5): 794–805. doi:10.1158/1535-7163.MCT-15-0003.

Applying Small Molecule Signal Transducer and Activator of Trancription-3 (STAT3) Protein Inhibitors as Pancreatic Cancer Therapeutics

Carolynn C. Arpin[1], **Stephen Mac**[1], **Yanlin Jiang**[2], **Huiwen Cheng**[2], **Michelle Grimard**[2], **Brent D. G. Page**[1], **Malgorzata M. Kamocka**[3], **Sina Haftchenary**[1], **Han Su**[4], **Daniel Ball**[1], **David A. Rosa**[1], **Ping-Shan Lai**[1], **Rodolfo F. Gómez-Biagi**[1], **Ahmed M. Ali**[1,5], **Rahul Rana**[1], **Helmut Hanenberg**[2,6,7], **Kagan Kerman**[4], **Kyle C McElyea**[8], **George E. Sandusky**[8], **Patrick T. Gunning**[1,*], and **Melissa L. Fishel**[2,9,*]

[1]Department of Chemistry, University of Toronto Mississauga, Mississauga, ON L5L 1C6, Canada

[2]Department of Pediatrics, Wells Center for Pediatric Research, Indiana University School of Medicine, Indianapolis, IN 46202

[3]Department of Medicine, Division of Nephrology, Indiana Center for Biological Microscopy, Indiana University School of Medicine, Indianapolis, IN 46202

[4]Department of Physical and Environmental Sciences, University of Toronto Scarborough, 1265 Military Trail, Toronto, ON M1C 1A4, Canada

[5]Department of Medicinal Chemistry, Faculty of Pharmacy, Assiut University, Assiut, Egypt

[6]Department of Pediatrics III, University Children's Hospital Essen, University of Duisburg-Essen, 45122 Essen, Germany

[7]Department of Otorhinolaryngology and Head/Neck Surgery (ENT) Heinrich Heine University, Dusseldorf, Germany

[8]Department of Pathology and Lab Medicine, Indiana University School of Medicine, Indianapolis, IN 46202

[9]Department of Pharmacology and Toxicology, Indiana University School of Medicine, Indianapolis, IN 46202

Abstract

Constitutively activated Signal Transducer and Activator of Transcription 3 (STAT3) protein has been found to be a key regulator of pancreatic cancer and a target for molecular therapeutic intervention. In this study PG-S3-001, a small molecule derived from the SH-4-54 class of STAT3 inhibitors, was found to inhibit patient-derived pancreatic cancer cell proliferation *in vitro* and *in vivo* in the low μM range. PG-S3-001 binds the STAT3 protein potently, K_d = 324 nM by SPR,

Corresponding authors: Melissa Fishel, 1044 W. Walnut Street, R4-321, Indianapolis, IN 46202; Tel: 317-274-8810; Fax: 317-274-8679; ; Email: mfishel@iu.edu. Patrick T. Gunning, Department of Chemistry, University of Toronto Mississauga, Mississauga, ON L5L 1C6, Canada; Tel: 905-828-5354; Fax: 905-828-5425; ; Email: patrick.gunning@utoronto.ca.

*Joint last authors.

The authors have no conflicts of interest to disclose.

showed no effect in a kinome screen (> 100 cancer-relevant kinases). *In vitro* studies demonstrated potent cell killing as well as inhibition of STAT3 activation in pancreatic cancer cells. To better model the tumor and its microenvironment, we utilized 3-Dimensional (3D) cultures of patient-derived pancreatic cancer cells in the absence and presence of cancer-associated fibroblasts (CAFs). In this co-culture model, inhibition of tumor growth is maintained following STAT3 inhibition in the presence of CAFs. Confocal microscopy was used to verify tumor cell death following treatment of 3D co-cultures with PG-S3-001. The 3D model was predictive of *in vivo* efficacy as significant tumor growth inhibition was observed upon administration of PG-S3-001. These studies showed that the inhibition of STAT3 was able to impact the survival of tumor cells in a relevant 3D model, as well as in a xenograft model using patient-derived cells.

Keywords

STAT3; three-dimensional culture; efficacy; transcription factor

Introduction

Approximately 25% of all deaths per year in the U.S. are caused by cancer, where pancreatic cancer is one of the most aggressive and lethal types (1). Patients face a one-year survival rate of 25% and a 5-year survival rate of only 6% (2). A proposed factor in the limited success of molecular therapies has been the heterogeneity found in pancreatic ductal adenocarcinoma (PDAC) samples pointing toward the need for strategies that target proteins that can affect multiple pathways (3–5). Lack of clinical efficacy is due, in part, to the desmoplastic fibrosis that accompanies pancreatic cancer (6, 7). The surrounding fibrotic network plays a principal role in supporting local tumor growth and distant metastasis (8–10). The challenge has been to identify the molecular effectors that critically regulate the survival of pancreatic cancer cells, to devise effective molecular-targeted strategies that can prevent or minimize the selection of resistant tumor variants, and then to penetrate the fibrotic nature of these tumors. Moreover, studies of stroma-specific depletion surprisingly found a decrease in survival rates of transgenic mouse models of pancreatic cancer attributing the loss of activated stroma to reduced survival (11, 12). As the contribution of the stroma is further investigated, future treatments for PDAC must be able to target the tumor in the presence of its associated microenvironment.

These studies address the role of Signal Transducer and Activator of Transcription 3 (STAT3) protein as a critical molecular target in pancreatic cancer. STAT3 is a transcription factor that regulates critical cell functions and has been implicated in several cancers, including breast, prostate, liver, and pancreas (13–15). In pancreatic cancer, STAT3 has been associated with cell proliferation and viability, as well as with angiogenesis and metastases (16–19). In genetically engineered mouse (GEMs) models of pancreatic cancer, STAT3 has been implicated in the establishment of early PDAC lesions (15, 20) as well as associated with tumor and stromal cell proliferation and resistance to gemcitabine therapy (21). STAT3 signaling is prevalent within the pancreatic tumor microenvironment as detailed herein. STAT3 activation can be regulated by several mechanisms, including phosphorylation and redox status (7, 22, 23). Several *in vitro* and *in vivo* studies using immortalized cells as well

as tumor cell lines showed that STAT3 blockade or inactivation (RNAi or pharmacological blockade) exerts inhibitory effects on the survival, proliferation, colony formation or invasiveness of human PDAC cells (24). Together, these results have identified STAT3 as an appealing target for therapeutic intervention (25–27).

STAT3 signaling (28) is initiated by extracellular cytokine/growth factor stimulation of a respective transmembrane protein, which results in the intracellular phosphorylation of key tyrosine (Y) residues. Cytokine binding to their cognate receptor leads to activation of a JAK (Janus kinase) protein, which then phosphorylates and activates cytoplasmic STAT3 protein. These phosphotyrosines (p-Y's) serve as docking sites for the Src Homology 2 (SH2) domain of STAT3, and once bound, STAT3 is phosphorylated on Y705. Phosphorylated STAT3 then dissociates and forms active homo-dimers via reciprocal binding of the SH2 domain of one protein and the p-Y705 of another. These transcriptionally-active dimers then translocate to the nucleus, bind to DNA, and promote target gene expression. While STAT3 activity is transient in healthy cells, it is often aberrant and constitutively active in cancer cells, including pancreatic cancer.

The STAT3 SH2 domain is integral to protein function. This shallow pocket binds transmembrane proteins, which enables STAT3 phosphorylation, activation, and formation of transcriptionally-active STAT3 homo-dimers (29). Previous efforts have focused on inhibiting STAT3 function by blocking the pY binding site within the SH2 domain (30) or the DNA binding domain. In general, STAT3 compounds have included peptidomimetics, (31, 32) oligonucleotides (33–35), metal complexes (36, 37), and small molecule inhibitors (38–43). Inhibitors operating via DNA binding domain blockade include inS3-54 (44) as well as Galeillalactone (45). Our efforts have focused on developing small molecule inhibitors of the SH2 domain: BP-1-102 (46, 47), BP-5-87 (48), and SH-4-54 (49). Unfortunately, only a small number of small molecule inhibitors for STAT3 protein have potencies and selectivity profiles suitable for advanced preclinical evaluation (26, 50). The discovery of a clinically relevant direct-binding STAT3 inhibitor has yet to be achieved. In this study, we sought to identify the most potent STAT3 inhibitors from a library of >100 salicylic and benzoic acid-based inhibitors, known to have STAT SH2 domain binding potential, and study the effects of these top-ranked analogs on PDAC tumor and stroma interactions.

Herein, we utilize state-of-the-art models, including 3D cultures of low passage patient-derived PDAC cells in the absence and presence of cancer-associated fibroblasts (CAFs) to better model the pancreatic tumor and its tumor microenvironment (TME) *in vivo.* Three-dimensional (3D) model systems more accurately mimic the complexity of cancer biology, compared to monolayer cell culture, and have the potential to provide relevant answers related to cancer treatment and disease specific, pancreatic cancer drug development (51, 52). Inhibition of tumor growth was observed following STAT3 inhibition as well as *in vivo* tumor efficacy studies. Blockade of STAT3 activity using BP-1-102, SH-4-54, and PG-S3-001 lead to PDAC cell death *in vitro* and tumor regression both in 3D co-culture systems and *in vivo* xenograft models of PDAC. Moreover, these studies showed that inhibition of STAT3 impacted the survival of tumor cells even in the presence of CAFs from the tumor

microenvironment. These studies support our hypothesis that STAT3 is a significant molecular target in PDAC.

Materials and Methods

Synthesis of STAT3 small molecules

All of the details of the chemistry for the library preparation and synthesis are contained in the Supplementary files. This file contains a detailed description of the synthesis as well as the characterization of lead compounds PG-S3-001, PG-S3-002, and PG-S3-003.

Cell lines and patient-derived PDAC cells

Pa03C, Panc10.05, Pa02C, and CAF19 were obtained from Dr. Anirban Maitra at The Johns Hopkins University (3). Upon receipt of the cells, we used STR (short tandem repeat) analysis (CellCheck with IDEXX BioResearch) to confirm that we indeed received the aforementioned cells from Dr. Maitra and we rechecked them via the same method in June 2015. Normal lung fibroblasts, CCD-13Lu and MIA-PaCa-2 were obtained from ATCC and were passaged for fewer than 6 months after resuscitation. All cells were maintained at 37 °C in 5% CO_2, grown in DMEM (Invitrogen; Carlsbad, CA) with 10% Serum (Hyclone; Logan, UT), and mycoplasma-free. The CAF19 cells were transduced with a lentivirus vector in order to make them stably express EGFP (enhanced green fluorescent protein) (53), and Pa03C cells were transduced with a lentivirus vector (pCL7TdTOMwo) in order to make them stably express TdTomato. CAF19 cells were seeded 24 h before 150 pfu/cell of the lentivirus was added to the media. One day later, the virus was removed; then cells were grown an additional 2 days in regular media.

Survival and proliferation studies

The proliferative capacity of PDAC and CAF19 cells as a monolayer was assessed using MTS tetrazolium dye assay as previously described (7). Using 96-well plates, we seeded either tumor cells alone (2,000–3,000 cell/well), CAFs alone (4,000 cell/well), or tumor + CAFs at a ratio of 2:1. STAT3 inhibitors were added 24 h after cells were seeded and MTS assay was performed 72 h later.

Three-dimensional Growth Assays

Ninety-six well plates were coated with 1% Noble Agar (Difco, 214220) in 10% serum containing media (50 μL/well) as described previously (54). Pa03C cells were re-suspended in normal growth media containing 3% Matrigel (BD Biosciences) at a cell density of 500 cells/well and plated on top of solidified 1% Noble Agar. Cells were treated on days 4 and 8 following plating with media containing 10% serum, 3% Matrigel, and STAT3 inhibitors. CellTracker dye (25 μM) or TdTomato via lentivirus was used to label these cells for confocal experiments to preserve the genetic characteristics of the low passage patient cells (3). The vehicle control was DMSO, was less than 0.01% of the volume, and was equivalent in each well. On Day 12, either Alamar blue reagent (LifeTechnologies) was added to each well (10μL/well) and incubated for 4 hr or spheroids were analyzed using Thermo ArrayScan high-content imaging system (55, 56). For Alamar blue assays, fluorescence reading at 544, 590 nM was then taken and used to assess survival following STAT3

inhibition. Images of 3D structures were captured by ArrayScan using a 2.5x objective for TdTomato and EGFP; then 2D projections were processed to quantify differences in total intensity and total area of both CAFs and tumor. After summarizing 4–5 repeats in both monolayer and 3D proliferation assays, we calculated effective dose-50 (ED_{50}s) for each compound using a line of best fit (i.e. linear regression model) where the percent survival equaled 50%.

Western blot analysis

Cells were harvested, lysed in RIPA buffer (Santa Cruz Biotechnology; Santa Cruz, CA), and protein was quantified and electrophoresed as previously described (7). Immunoblotting was performed using the following antibodies: total STAT3, and p-STAT3(p-Y705) (Cell Signaling; Danvers, MA) at a 1:1000 dilution.

Imaging of 3-Dimensional Spheres

In order to visualize the tumor cells for imaging of the structure, we labeled the Pa03C cells with CellTracker fluorescent probe (Invitrogen, C34552). We incubated the cells with 25 μM probe for 45 min in serum free media, then we spun down the cells, and let them recover in media containing serum for 30 min at 37 °C. CAFs utilized in these experiments stably express EGFP as described above. We imaged the cells on Days 5 and 11 to capture the effect of STAT3 inhibition in the middle and end of the 3D assay. On Day 11, we added Alamar blue to the wells to confirm the decrease in proliferation visualized by the confocal fluorescent imaging.

Confocal images of spheres were acquired with a confocal/two-photon Olympus Fluoview FV-1000 MPE system (Olympus America, Central Valley, PA) available at the Indiana Center for Biological Microscopy (ICBM) facility (Indianapolis, IN), using an Olympus UMPLFL 10X W NA:0.30 air objective and XLUMPLFL 20X water NA:0.95 lenses. Images were collected at 512×512 frame size, 8 μs pixel dwell time, and in a sequential illumination mode using 488- and 559-nm excitation laser lines. Emission light was collected with two spectral detectors set up at 500–545 nm and 570–670 nm filter ranges. Due to the large size and density of the control and vehicle-treated spheres, accurate visualization of the entire sphere using confocal scanning mode was not possible on Day 11. It was hypothesized that this was due to compromised light penetration through the tightly packed spheres. Therefore, transmitted light images were collected simultaneously with confocal scans to evaluate overall size for the spheres. Axial scanning (Zstack) was performed, optical consecutive and parallel slices were collected using optimal step size. Maximum intensity projection (MIP) images were created out of collected image data stacks using Olympus Fluoview Image Viewer v.3.0. 3D reconstruction images were created out of collected image data stacks using Amira software (FEI Co., Hillsboro, OR).

In vivo efficacy of STAT3 inhibitors in low passage patient-derived cells

All studies were carried out in accordance with, and approval of, the Institutional Animal Care and Use Committee of Indiana University Medical School, and the Guide for the Care and Use of Laboratory Animals. Male and female NOD.Cg-*Prkdc*^{scid}*Il2rg*^{tm1Wjl}/SzJ (common name NSG) mice were obtained from the *In Vivo* Therapeutics Core of the

Indiana University Simon Cancer Center. Animals were housed under pathogen-free conditions and maintained on Teklad Lab Animal Diet (P/N TD 2014, Harlan Laboratories USA) with *ad libitum* access to sterile tap water under a 12-hour light-dark cycle at 22–24 °C. Using low passage patient-derived cells, Pa03C, ectopic xenografts were grown in NSG mice. Pa03C cells (2.5×10^6 cells/mouse) in 0.2 ml of DMEM media:Matrigel (50:50) were implanted subcutaneously (s.c.) into the right flanks of NSG mice. Compound PG-S3-001 was dissolved in 4% CremophorEL:EtOH (1:1) / saline solution. When tumor volumes were 71±4 mm^3, compound PG-S3-001 was administered once daily at 10 mg/kg for 15 days intrapertitoneal (ip). Mice were weighed twice weekly to assess toxicity. Tumors were measured weekly during treatment. Tumor volumes were monitored by caliper measurement [tumor volume = length × (perpendicular width)^2 × 0.5] and the average tumor volume in mm^3 for each treatment group was plotted. Treatment started on day 8 post-implant. Average tumor volume ± SE for the vehicle (n=18) and PG-S3-001-treated (n=16) xenografts was analyzed by student's t test. On day 25, the mice were sacrificed and the tumors excised and weighed.

Immunohistochemistry of tumor tissue

Tissues were fixed overnight at room temperature in 10% NBF after which they were transferred through graded concentrations of alcohol to xylene inside a Leica Automated Vacuum Tissue Processor. Tissues were embedded in paraffin before being cut into 5 micron thick sections, mounted onto positively charged slides, and baked at 60°C. The slides were then deparaffinized in xylene and rehydrated through graded alcohols to water. Antigen retrieval was performed by immersing the slides in a Target Retrieval Solution (Dako) for 20 min. at 90°C. (in a water bath), cooling at room temperature for 10 min., washing in water and then proceeding with immunostaining. Slides were blocked with protein blocking solution (Dako) for 30 mins. All subsequent staining steps were performed using the Dako FLEX SYSTEM on an automated Immunostainer; incubations were done at room temperature and Tris buffered saline plus 0.05% Tween 20, pH 7.4 (TBS - Dako Corp.) was used for all washes and diluents. The primary antibodies were anti-mouse phospho-Histone H3 (1:500, Dako) and p-STAT3 (1:25, Cell Signaling). Control sections were treated with an isotype control using the same concentration as primary antibodies to verify the staining specificity. The Aperio whole slide digital imaging system was used for imaging. The Aperio ScanScope CS system was used (360 Park Center Drive Vista, CA 92081). The system imaged all slides at 20x. Slides were reviewed by two pathologists, and tissue was recorded as % tumor, % necrosis, % inflammation, and % stroma. The pathology hand count was only evaluated in an area of viable tumor cells. An average of mitotic figures (at x20) were hand-counted from four hot-spot areas on each tissue. The control and treatment groups were then evaluated for statistical differences.

Determination of inhibitory constants for small-molecules using Fluorescence Polarization (FP) assays

Competitive binding FP assays were performed for the lead inhibitors PG-S3-001, PG-S3-002, and PG-S3-003 against STAT3 protein. The assays were performed in flat black 384-well plates (Corning #3573) and FP measurements were taken with the Infinite M1000 machine (Tecan, Crailsheim, Germany). The buffer conditions for all assays were 10 mM

HEPES, 50 mM NaCl, 1 mM EDTA, 2 mM TCEP, pH 7.5 and the final DMSO concentration in the wells was kept constant at 10%. Calibration curves for the wildtype STAT3 proteins were derived by incubating a 10 nM final concentration of a fluoresceinated-phosphopeptide (5-FAM-GpYLPQTV for STAT3), with increasing concentrations of protein. The point at which 80% of the fluoresceinated-phosphopeptide was bound was used as the optimal protein concentration required for the competitive FP assays. For the STAT3 FP assays, the 5-FAM-GpYLPQTV-NH_2 peptide and STAT3 protein were incubated for 30 min. at room temperature. Inhibitors were titrated at concentrations ranging from 1 nM to 500 μM and incubated for a further 15 min. at which point FP measurements were taken in triplicate. The final well concentrations of the fluoresceinated-phosphopeptide and STAT3 protein were 10 nM and 250 nM, respectively. FP measurements were normalized and plotted against inhibitor concentration on a logarithmic scale. The raw data was fitted with a standard dose-normalized response inhibition curve using GraphPad Prism 6 software. All inhibitory constants and K_i values are summarized in Fig 2 (57).

Surface Plasmon Resonance (SPR) Spectroscopy

SPR binding experiments were performed using a ProteOn™ XPR36 (Bio-Rad Laboratories Ltd.). ProteOn™ HTE sensor chips (#176-5033) that had an elevated tris-NTA surface density optimal for protein-small molecule interactions were used in connection with ProteOn HTE capturing kit. The horizontal and vertical spots of the sensor chips were conditioned using consecutive injections of 0.5% SDS, 50 mM NaOH, 100 mM HCl followed by 300 mM EDTA for 1 min. each at a flow rate of 30 μL/min. Then, the sensor chips were activated using 10 mM $NiSO_4$ for 2 min. in the horizontal orientation at a flow rate of 30 μL/min. Immediately after the activation step, His-tagged STAT3 (0.5 – 25 μg/mL, SignalChem, Richmond, BC) protein was immobilized until the desired ligand immobilization level of ~12 kRU was obtained at a flow rate of 30 μL/min. Small molecules were injected at various concentrations both in vertical (control spots with no protein) and horizontal (protein-immobilized spots) orientations at a flow rate of 5 μL/min. To determine the full kinetic profile, small molecule-protein binding spectrograms were evaluated using the ProteOn™Manager software.

Docking of inhibitors to STAT3 and visualization of the computed receptor-ligand complex

Ligand structures were modeled and the geometry optimized in Maestro 9.9 (Schrödiner Suite). The STAT3 crystal structure in complex with DNA (PDB ID:1Y1U) was imported in Maestro where water molecules and the DNA oligonucleotides were removed. Hydrogen atoms were added followed by assigning Gasteiger charges to the receptor. Molecular docking simulations were performed with Glide 6.5 using a receptor grid localized within the STAT3 SH2 domain. Simulation results were analyzed using Pose Viewer and imported to MacPyMol v.1.7.6. Molecular docking protocols are outlined in the supporting information (57–59).

qPCR Off-Target Screening for Kinome Activity

A competitive qPCR screening was employed to identify off-target activity of PG-S3-001 against a comprehensive DiscoveRx *KINOMEscan* library of 132 human kinases. In this assay, kinases labeled with DNA were treated with PG-S3-001 (5 μM single concentration)

and incubated with an immobilized ligand designed to capture its target kinase. Ultra-sensitive quantitative PCR (qPCR) is employed to measure levels of immobilized kinases when treated with PG-S3-001 and relative kinase levels compared to control samples. In this screen, hits are classified as compounds where captured kinase levels fall below a 30% threshold. Images were generated using TREEspot software tool and reprinted with permission from KINOMEscan, a division of DiscoveRx Corporation. Results pertaining to the interaction of PG-S3-001 with relevant kinases is included in the Supplementary files (Supplementary Table 1).

Results

Screening of novel STAT3 inhibitors in patient-derived pancreatic cancer cell lines

To identify compounds best suited for targeting p-STAT3 in PDAC cell lines, we conducted a screen of 52 salicylic and benzoic acid containing compounds prepared in our lab with demonstrated anti-cancer activity on p-STAT3-containing tumor cell lines. In total, 52 compounds (including a range of previously published inhibitors) were screened using a cell viability assay employing low passage patient-derived cells, Panc10.05. Previous work demonstrated that both these cells and the additional patient derived cells (Pa03C) used here, express p-STAT3 and can be killed following inhibition of p-STAT3 (7). This initial screen revealed that three of the newly synthesized derivatives PG-S3-001, PG-S3-002, and PG-S3-003 (Fig. 1A) were more potent than, BP-1-102. For our proliferation assays, BP-1-102 and SH-4-54 were utilized as comparator parent compounds (Fig. 1B, C). Specifically, PG-S3-001 and PG-S3-002 displayed enhanced efficacy against PDAC cells, with respective ED_{50} values of 2.4 ± 0.2μM and 3.0 ± 0.1μM (Fig. 1C). PG-S3-003 was less effective than PG-S3-001, PG-S3-002, and SH-4-54 at blocking proliferation of Panc10.05 cells, with an ED_{50} value of 18.7 ± 1.1μM for PG-S3-003 and 8.7 ± 1.9 μM for SH-4-54 (Fig. 1C). In the case of PG-S3-003, the valine linker afforded a modest increase in potency over parent compound, BP-1-102. A similar trend was observed with SH-4-54's congener, PG-S3-001 (Fig. 1B), where an approximate 3-fold enhancement in activity was observed. The increase in potency could be attributed to valine acting as a conformational lock; restricting the number of accessible conformations and decreasing the entropic cost of binding to STAT3.

Predictive computational modeling of PG-S3-001 to the SH2 domain of STAT3: analysis of ligand-receptor interaction

The initial lead STAT3 inhibitors, BP-1-102 and SH-4-54 both possess a relatively flexible glycine core. The conformational effect of the bulkier isopropyl alkyl appendage of PG-S3-001 was investigated *in silico* using the molecular docking software, Glide 6.5 (Schrödinger Suite). As previously reported, BP-1-102 and SH-4-54, which differ only by a phenolic hydroxide, have essentially identical structural orientation and energetic contacts with STAT3 (49). Comparative docking within the SH2 domain of PG-S3-001 is shown in Fig. 2A. It revealed analogous electrostatic interactions between the carboxylate group of the inhibitor with the positively charged and hydrophilic pY-recognition pocket consisting of Arg609, Ser611, Ser613 and Lys591. The cyclohexylbenzyl appendage of PG-S3-001 projects towards Glu638 whereas the pentafluorobenzene of PG-S3-001 was shown to adopt a different conformation relative to both SH-4-54 and BP-1-102. As seen from Fig. 2A and a

two-dimensional interaction map (Fig. 2B), the pentafluorobenzne group forms dipolar interaction with the backbone carbonyl oxygen of Pro715 and favourable hydrophobic contact with Phe716. Finally, it was observed that PG-S3-001 adopts a conformation such that the isopropyl appendage interacts with the alkyl side chain of Ile634.

Measuring inhibitor binding to STAT3 protein

With three lead compounds in hand, two biophysical techniques were used to assess inhibitor binding to the STAT3 protein. First, a fluorescence polarization (FP) assay was employed to measure the disruption of the native p-STAT3 SH2 domain complex in the presence of inhibitor as an initial gauge of binding affinity. The lead compounds, PG-S3-001, PG-S3-002, and PG-S3-003 demonstrated modest binding affinities to STAT3 protein (K_i = 72 ± 6 μM, 45 ± 7μM, and 39 ± 3 μM, respectively; Fig. 3A).

Second, SPR spectroscopy was used to determine the K_d (k_{on}/k_{off}) values for PG-S3-001 and PG-S3-002 against STAT3. Calculated K_d's for PG-S3-001 and PG-S3-002 were 324 ± 37 nM and 301 ± 32 nM, respectively (Fig. 3B), which were comparable to that of parent compound SH-4-54 (300 ± 27 nM). It can be seen from the SPR traces that both compounds appear to have either slow dissociative off-rates (k_{off}), suggesting longer target–drug residence times, or are irreversible inhibitors. For example, it is possible that PG-S3-001 is alkylating the STAT3 protein through cysteine mediated nucleophilic aromatic substitution at the *para*-arylfluoride position of the pentafluorobenzene. The difference in activity relative to the FP data is likely explained by PG-S3-001 binding to a region of STAT3 other than the SH2 domain. This postulated mechanism of action will be investigated in future studies. However, given the Panc10.05 cell viability and biophysical data, PG-S3-001 was selected as the lead compound.

Lead STAT3 inhibitor effectively disrupts PDAC and CAF cell survival and proliferation individually and in co-culture

In addition to the tumor cell proliferation studies in Fig. 1, additional validating studies in low passage patient derived cell line, Pa03C, were performed. The cytotoxicity of PG-S3-001 was evaluated in the MTS assay in these cells (Fig. 4A), cancer associated fibroblasts (CAF19, Fig. 4B) and in a 2:1 co-culture (Fig. 4C) to determine its cellular efficacy. In all three cultures, PG-S3-001 (IC_{50} = 3.7 ± 0.4 μM, tumor cells; 4.0 ± 0.7 μM, CAFs; 4.7 ± 0.1 μM, co-culture) exceeded the performance of parent compounds BP-1-102 (IC_{50} = 19.1 ± 0.9 μM, tumor cells; 15.2 ± 2.7 μM CAFs; 16.4 ± 0.6 μM co-culture) and SH-4-54 (IC_{50} = 9.2 ± 1.7 μM tumor cells; 7.6 ± 0.9 μM CAFs; 11.8 ± 1.1 μM co-culture) at concentrations below their half maximal inhibition concentration (IC_{50}s). Furthermore, cell proliferation was monitored using normal human lung fibroblasts, CCD-13Lu following STAT3 inhibition. It has been previously shown that STAT3 inhibition is more cytotoxic to cancer cells as compared to normal cells; therefore, primary, normal fibroblasts, CCD-13Lu were included to demonstrate that the cytotoxicity observed following inhibition of STAT3 was preferential to tumor cells and activated fibroblasts (Fig. 4D). After incubation for 72 h, PG-S3-001 severely impaired the growth of Pa03C and CAF19 cells, whereas the primary CCD-13Lu cell line retained 84% of its relative growth. Compared to parent compounds, PG-S3-001 exhibited superior efficacy (~10-fold) for mitigating growth of the patient

derived adenocarcinoma Pa03C cells. When comparing the three compounds in CAF19 cells, the activity of PG-S3-001 is, within error, comparable to BP-1-102 and SH-4-54.

STAT3 inhibitors decrease STAT3 phosphorylation

Treatment with BP-1-102, SH-4-54, and PG-S3-001 inhibited phosphorylation of STAT3 at Y705 (Fig. 4E) as well as cellular proliferation in PDAC cells, CAFs, and co-cultures (Fig. 4A–C). Inhibition of STAT3 activity correlated well to the amount of cell killing by our lead compounds. In Fig. 4E, concentration of parent compounds BP-1-102 and SH-4-54 was 10 μM and PG-S3-001 was 5μM. The amount of inhibition of STAT3 activity via levels of p-STAT3 correlated with the amount of cell killing of each of these compounds: PG-S3-001 > SH-4-54 > BP-1-102. PG-S3-001 can significantly inhibit dose-dependent activation of STAT3 at Y705 in two additional PDAC cell lines, established cell line MIA-PaCa-2 and low passage patient derived line Pa02C (Figure 4F, PaCa-2, $p<0.05$, comparing IL-6 control with 5μM and $p<0.01$ with 10μM PG-S3-001 and Pa02C, $p<0.01$ (IL-6 control vs 5 μM and $p<0.001$ for IL-6 control vs 10μM). The activation of p-STAT3 is also dramatically blocked in the CAF cells as shown in Figure 4G. This blockade of STAT3 in the CAFs led to >60% down-regulation of STAT3 regulated gene, survivin in the CAF cells as well ($p<0.01$).

Lead compound PG-S3-001 does not significantly inhibit upstream kinases as assessed by a kinome screen

To probe for off-target effects, PG-S3-001 (5 μM concentration) was submitted to a kinome screen against 132 different kinases. PG-S3-001 exhibited minimal affinity for kinases directly involved in STAT3 phosphorylation. Only proto-oncogene SRC kinase was moderately inhibited (36 % inhibition at 5 μM, Supplementary Information, Table 1). These data further validated PG-S3-001 as a candidate for the 3D tumor model and *in vivo* efficacy studies.

Inhibition of p-STAT3 inhibits cell growth in three-dimensional culture systems

State-of-the-art three-dimensional (3D) culture systems (54) in the presence and absence of CAFs were utilized to further screen our lead compound for efficacy at killing PDAC cells. 3D tumor-stromal cell-associated spheroid models (Fig. 5) include selective pressures akin to the TME which has several advantages over traditional monolayer cell culture (51, 52, 60, 61). CAF cells isolated from a pancreatic cancer patient (62) were included to recapitulate a more accurate picture of cell-cell interactions *in vivo* (Fig. 5). Due to the importance of the stroma in this disease (51, 52), CAFs and tumor cells were labeled in order to assess which cell type in the 3D co-culture was most effected by STAT3 inhibition. As expected, co-culture of CAFs with tumor cells increased the growth of tumor spheres (Fig. 5). Inhibition of p-STAT3 via BP-1-102, SH-4-54, and PG-S3-001 resulted in inhibition of growth in 3D as was also observed with monolayer cell cultures. Inhibition of STAT3 was found to effectively slow the growth rate of cells in a dose-dependent manner (Fig. 5A–C), with IC_{50}'s ranging from ~15.2 – 27.0 μM in 3D culture and ~23.5 – 42.5 μM for 3D culture containing tumor and CAFs. As expected, PDAC cells grown in 3D as well as the addition of CAFs to the 3D cultures resulted in an increase in resistance to STAT3 inhibition. However, in this assay, PG-S3-001 (IC_{50} = 15.2 ± 2.0 μM, tumor and 23.5 ± 4.4 μM, co-culture) was more potent than the parent compounds, even in the presence of stromal CAFs

(Fig. 5C). The data in Figure 5A–C was generated using a proliferation-based Alamar blue assay which provided reliable information about the effects of the compounds on the proliferation of both cell types but does not delineate which cell type was affected by inhibition of STAT3 activity. Therefore, we used two additional methods to quantitate and visualize the effects of PG-S3-001 on PDAC cells alone and in co-culture.

Two-dimensional projections of 3D images captured by ArrayScan high-content screening system were used to quantitate the area and relative intensity (RLU) of the red and green channels. Both the tumor cells alone and in co-culture are sensitive to the STAT3 inhibitor, PG-S3-001 as evidenced by a dose-dependent decrease in area and intensity (Figure 5D, E). As shown in Figure 5D, the area of the tumor spheroids is more dramatically affected by the PG-S3-001 compound than the area of the CAFs ($p<0.01$ comparing the area of the tumor to the area of the CAFs). The fluorescent intensity of both tumor cells and CAFs was decreased following treatment (Figure 5E). The CAFs provide significant protection to the tumor cells as there are significant differences between the tumor alone and the tumor in co-culture both in area and intensity (Figure 5D, E).

Confocal microscopy further demonstrates the decrease in viability of PDAC cells following p-STAT3 inhibition

Confocal microscopy confirms the results from the high content imaging system demonstrating enhanced effects of the PG-S3-001 STAT3 inhibitor on tumor proliferation (Figure 5F,G). At days 5 and 11 after treatment, confocal images were acquired to confirm the presence of both cell types in the spheres as well as the effects of PG-S3-001 on both cell types (Fig. 5F,G). At Day 11, transmitted light images were acquired simultaneously with confocal images. Both CAFs (green signal) and tumor cells (red signal) decreased following treatment with PG-S3-001, but tumor cell intensity was more drastically reduced at Day 5. Again, the confocal microscopy data confirmed that the tumor cells appeared to be more sensitive to the inhibition of STAT3 than the CAFs since EGFP fluorescence persists. Based on recent data, which suggests that depletion of the stroma in PDAC is not beneficial to the patient and can accelerate the disease (11, 12), it is important to understand the effects of p-STAT3 inhibition in both cell types when they are co-cultured and interacting. When analyzed in 3D co-culture, encouragingly, based on EGFP fluorescent readout, the CAF cells are still present following treatment with STAT3 inhibitors (Fig. 5D–G), suggesting a promising selectivity profile. Since PG-S3-001 effectively inhibited p-STAT3 activity and blocked proliferation in traditional cell culture models, as well as in 3D models, PG-S3-001 was next assessed in an *in vivo* model.

3D co-culture assay predicts the in vivo efficacy of a potent STAT3 inhibitor on pancreatic cancer xenografts

A patient-derived xenograft (PDX) model was utilized to demonstrate that STAT3 inhibitor, PG-S3-001 was effective as a single agent. After tumors from patient-derived cells, Pa03C reached an average of 71 ± 4 mm^3, treatment with PG-S3-001 was initiated (ip, 10 mg/kg). PG-S3-001 was not overly toxic to the animals as measured by weight loss (Fig. 6A). In contrast to vehicle-control tumors, patient-derived xenografts demonstrated a significant tumor growth delay (54–62 %) after treatment with PG-S3-001 for 15 days (Fig. 6B). To

further confirm the mechanism of action of PG-S3-001, immunohistochemistry was conducted to quantitate the levels of activated STAT3 (p-Y705) and found a 45 % reduction in the levels of activated STAT3 following treatment with PG-S3-001 (Fig. 6C). The tumor growth delay also resulted in a significantly smaller tumor weight. Tumor weight was 36 % lower in PG-S3-001-treated mice compared to vehicle-treated mice when weighed at the conclusion of the study (Fig. 6D). The antitumor effect is at least partially due to a reduction in cell proliferation as we observed a significant decrease in phospho-histone H3, a marker of mitotic cells (63) in tumors treated with PG-S3-001. The preclinical results suggested that targeting STAT3 in PDAC might have clinical efficacy and further confirmed that the 3D co-culture model is predictive of *in vivo* efficacy.

Discussion

Novel models were used to characterize a new class of STAT3 inhibitors, including low passage patient-derived cells and 3D co-culture systems to address the role of the TME. 3D tumor-stromal cell-associated spheroid models in Figure 5 include both tumor and CAFs to better model PDAC *in vitro*. This has several advantages over traditional monolayer cell culture (51, 52, 60, 61). Monolayers are grown on stiff polystyrene plastic, while 3D culture systems are grown as floating tumor spheroids allowing for diffusion of nutrients similar to human tumors (54). Additionally, spheroids provide a more accurate portrayal of tumors *in vivo* due to the altered proliferation and morphology in 3D and the increased length of time for culturing when compared to traditional monolayer techniques. CAF cells from the TME were included to recapitulate a more accurate picture of cell-cell interactions *in vivo* (Fig. 5). The sensitivity of CAF cells to STAT3 inhibition was similar to tumor cells in monolayer; however, in 3D co-culture we observed promising selectivity for inhibition of tumor cell proliferation that again speaks to the relevance of the *in vitro* 3D model.

In summary, we have reported the use of a low μM p-STAT3 inhibitor to selectively target patient-derived pancreatic cancer cells in the presence of CAFs, and provided preliminary preclinical evidence to suggest that p-STAT3 inhibition might afford an effective therapy for pancreatic cancer patients. While more potent and selective p-STAT3 inhibitors are required to realize this goal, the described 3D PDAC tumor model provides a more realistic model of the disease for screening potential STAT3 inhibitors. For example, in co-culture with CAFs, compound activity, relative to that observed in monolayer PDAC cell culture, drops significantly. Thus, inhibitors that can selectively target 3D PDAC tumor cells in stroma will likely have better efficacy in preclinical models. As demonstrated, this 3D model approach will serve as a most useful screening tool as we seek to discover new and more effective regimens for treating pancreatic cancer.

Supplementary Material

Refer to Web version on PubMed Central for supplementary material.

Acknowledgments

This work was supported by grants from the National Institutes of Health, NCI CA167291 to M.L. Fishel with additional support from the IUSCC ITRAC basic science pilot funding mechanism, Indiana Clinical Translational

Science Institute, Project Development Team within the ICTSI NIH/NCRR Grant Number UL1TR001108 to M.L. Fishel. M.L. Fishel supported in part by Jeff Gordon Children's Foundation. CIHR, Leukemia and Lymphoma Society, Canada Research Chair Program, Alberta Innovates, and Canadian Foundation for Innovation to P.T. Gunning. A MITACS post-doctoral fellowship supported R.F. Gomez-Biagi.

We thank Drs. Murray Korc and Jesse Gore, Department of Medicine for help with establishing the three-dimensional culture assay.

References

1. Statistics CNCfH. National Center for Health Statistics; 2014.
2. Society AC. Cancer Facts and Figures. 2011.
3. Jones S, Zhang X, Parsons DW, Lin JC, Leary RJ, Angenendt P, et al. Core signaling pathways in human pancreatic cancers revealed by global genomic analyses. Science. 2008; 321:1801–6. [PubMed: 18772397]
4. Biankin AV, Waddell N, Kassahn KS, Gingras MC, Muthuswamy LB, Johns AL, et al. Pancreatic cancer genomes reveal aberrations in axon guidance pathway genes. Nature. 2012; 491:399–405. [PubMed: 23103869]
5. Makohon-Moore A, Brosnan JA, Iacobuzio-Donahue CA. Pancreatic cancer genomics: insights and opportunities for clinical translation. Genome medicine. 2013; 5:26. [PubMed: 23673020]
6. Erkan M, Reiser-Erkan C, Michalski CW, Kleeff J. Tumor microenvironment and progression of pancreatic cancer. Exp Oncol. 2010; 32:128–31. [PubMed: 21403605]
7. Cardoso AA, Jiang Y, Luo M, Reed AM, Shahda S, He Y, et al. APE1/Ref-1 Regulates STAT3 Transcriptional Activity and APE1/Ref-1-STAT3 Dual-Targeting Effectively Inhibits Pancreatic Cancer Cell Survival. PLoS ONE. 2012; 7:e47462. [PubMed: 23094050]
8. Apte MV, Park S, Phillips PA, Santucci N, Goldstein D, Kumar RK, et al. Desmoplastic reaction in pancreatic cancer: role of pancreatic stellate cells. Pancreas. 2004; 29:179–87. [PubMed: 15367883]
9. Pietras K, Ostman A. Hallmarks of cancer: interactions with the tumor stroma. Exp Cell Res. 2010; 316:1324–31. [PubMed: 20211171]
10. Xie D, Xie K. Pancreatic cancer stromal biology and therapy. Genes Dis. 2015; 2:133–43. [PubMed: 26114155]
11. Ozdemir BC, Pentcheva-Hoang T, Carstens JL, Zheng X, Wu CC, Simpson TR, et al. Depletion of carcinoma-associated fibroblasts and fibrosis induces immunosuppression and accelerates pancreas cancer with reduced survival. Cancer Cell. 2014; 25:719–34. [PubMed: 24856586]
12. Rhim AD, Oberstein PE, Thomas DH, Mirek ET, Palermo CF, Sastra SA, et al. Stromal elements act to restrain, rather than support, pancreatic ductal adenocarcinoma. Cancer Cell. 2014; 25:735–47. [PubMed: 24856585]
13. Yu H, Jove R. The STATs of cancer--new molecular targets come of age. Nat Rev Cancer. 2004; 4:97–105. [PubMed: 14964307]
14. Lesina M, Wormann SM, Neuhofer P, Song L, Algul H. Interleukin-6 in inflammatory and malignant diseases of the pancreas. Seminars in immunology. 2014; 26:80–7. [PubMed: 24572992]
15. Corcoran RB, Contino G, Deshpande V, Tzatsos A, Conrad C, Benes CH, et al. STAT3 plays a critical role in KRAS-induced pancreatic tumorigenesis. Cancer Res. 2011; 71:5020–9. [PubMed: 21586612]
16. Xie K, Wei D, Huang S. Transcriptional anti-angiogenesis therapy of human pancreatic cancer. Cytokine Growth Factor Rev. 2006; 17:147–56. [PubMed: 16516532]
17. Li H, Huang C, Huang K, Wu W, Jiang T, Cao J, et al. STAT3 knockdown reduces pancreatic cancer cell invasiveness and matrix metalloproteinase-7 expression in nude mice. PLoS ONE. 2011; 6:e25941. [PubMed: 21991388]
18. Fofaria NM, Srivastava SK. STAT3 induces anoikis resistance, promotes cell invasion and metastatic potential in pancreatic cancer cells. Carcinogenesis. 2015; 36:142–50. [PubMed: 25411359]
19. Devarajan E, Huang S. STAT3 as a central regulator of tumor metastases. Curr Mol Med. 2009; 9:626–33. [PubMed: 19601811]

20. Lesina M, Kurkowski MU, Ludes K, Rose-John S, Treiber M, Kloppel G, et al. Stat3/Socs3 activation by IL-6 transsignaling promotes progression of pancreatic intraepithelial neoplasia and development of pancreatic cancer. Cancer Cell. 2011; 19:456–69. [PubMed: 21481788]
21. Nagathihalli NS, Castellanos JA, Shi C, Beesetty Y, Reyzer ML, Caprioli R, et al. Signal Transducer and Activator of Transcription 3, Mediated Remodeling of the Tumor Microenvironment Results in Enhanced Tumor Drug Delivery in a Mouse Model of Pancreatic Cancer. Gastroenterology. 2015; 149:1932–43. e9. [PubMed: 26255562]
22. Bhakat KK, Mantha AK, Mitra S. Transcriptional Regulatory Functions of Mammalian AP-endonuclease (APE1/Ref-1), an Essential Multifunctional Protein. Antioxid Redox Signal. 2009; 11:621–38. [PubMed: 18715144]
23. Li L, Cheung SH, Evans EL, Shaw PE. Modulation of gene expression and tumor cell growth by redox modification of STAT3. Cancer Res. 2010; 70:8222–32. [PubMed: 20807804]
24. Yu H, Lee H, Herrmann A, Buettner R, Jove R. Revisiting STAT3 signalling in cancer: new and unexpected biological functions. Nat Rev Cancer. 2014; 14:736–46. [PubMed: 25342631]
25. Siveen KS, Sikka S, Surana R, Dai X, Zhang J, Kumar AP, et al. Targeting the STAT3 signaling pathway in cancer: role of synthetic and natural inhibitors. Biochim Biophys Acta. 2014; 1845:136–54. [PubMed: 24388873]
26. Lavecchia A, Di Giovanni C, Cerchia C. Novel inhibitors of signal transducer and activator of transcription 3 signaling pathway: an update on the recent patent literature. Expert opinion on therapeutic patents. 2014; 24:383–400. [PubMed: 24432979]
27. Haftchenary S, Avadisian M, Gunning PT. Inhibiting aberrant Stat3 function with molecular therapeutics: a progress report. Anticancer Drugs. 2011; 22:115–27. [PubMed: 21063201]
28. Aaronson DS, Horvath CM. A road map for those who don't know JAK-STAT. Science. 2002; 296:1653–5. [PubMed: 12040185]
29. Darnell JE Jr. STATs and gene regulation. Science. 1997; 277:1630–5. [PubMed: 9287210]
30. Kraskouskaya D, Duodu E, Arpin CC, Gunning PT. Progress towards the development of SH2 domain inhibitors. Chem Soc Rev. 2013; 42:3337–70. [PubMed: 23396540]
31. McMurray JS, Mandal PK, Liao WS, Ren Z, Chen X. Inhibition of Stat3 by cell-permeable peptidomimetic prodrugs targeted to its SH2 domain. Adv Exp Med Biol. 2009; 611:545–6. [PubMed: 19400306]
32. Mandal PK, Limbrick D, Coleman DR, Dyer GA, Ren Z, Birtwistle JS, et al. Conformationally constrained peptidomimetic inhibitors of signal transducer and activator of transcription. 3: Evaluation and molecular modeling. J Med Chem. 2009; 52:2429–42. [PubMed: 19334714]
33. Leong PL, Andrews GA, Johnson DE, Dyer KF, Xi S, Mai JC, et al. Targeted inhibition of Stat3 with a decoy oligonucleotide abrogates head and neck cancer cell growth. Proc Natl Acad Sci U S A. 2003; 100:4138–43. [PubMed: 12640143]
34. Xi S, Gooding WE, Grandis JR. In vivo antitumor efficacy of STAT3 blockade using a transcription factor decoy approach: implications for cancer therapy. Oncogene. 2005; 24:970–9. [PubMed: 15592503]
35. Sen M, Thomas SM, Kim S, Yeh JI, Ferris RL, Johnson JT, et al. First-in-human trial of a STAT3 decoy oligonucleotide in head and neck tumors: implications for cancer therapy. Cancer discovery. 2012; 2:694–705. [PubMed: 22719020]
36. Drewry JA, Fletcher S, Yue P, Marushchak D, Zhao W, Sharmeen S, et al. Coordination complex SH2 domain proteomimetics: an alternative approach to disrupting oncogenic protein-protein interactions. Chemical communications. 2010; 46:892–4. [PubMed: 20107641]
37. Auranofin and auranofin analogs useful to treat proliferative disease and disorders: Board regent. 2012.
38. Fletcher S, Singh J, Zhang X, Yue P, Page BD, Sharmeen S, et al. Disruption of transcriptionally active Stat3 dimers with non-phosphorylated, salicylic acid-based small molecules: potent in vitro and tumor cell activities. Chembiochem. 2009; 10:1959–64. [PubMed: 19644994]
39. Song H, Wang R, Wang S, Lin J. A low-molecular-weight compound discovered through virtual database screening inhibits Stat3 function in breast cancer cells. Proc Natl Acad Sci U S A. 2005; 102:4700–5. [PubMed: 15781862]

40. Suganami E, Takagi H, Ohashi H, Suzuma K, Suzuma I, Oh H, et al. Leptin stimulates ischemia-induced retinal neovascularization: possible role of vascular endothelial growth factor expressed in retinal endothelial cells. Diabetes. 2004; 53:2443–8. [PubMed: 15331557]
41. Siddiquee K, Zhang S, Guida WC, Blaskovich MA, Greedy B, Lawrence HR, et al. Selective chemical probe inhibitor of Stat3, identified through structure-based virtual screening, induces antitumor activity. Proc Natl Acad Sci U S A. 2007; 104:7391–6. [PubMed: 17463090]
42. Shahani VM, Ball DP, Ramos AV, Li Z, Spagnuolo PA, Haftchenary S, et al. A 2,6,9-hetero-trisubstituted purine inhibitor exhibits potent biological effects against multiple myeloma cells. Bioorg Med Chem. 2013; 21:5618–28. [PubMed: 23810672]
43. Ashizawa T, Miyata H, Ishii H, Oshita C, Matsuno K, Masuda Y, et al. Antitumor activity of a novel small molecule STAT3 inhibitor against a human lymphoma cell line with high STAT3 activation. Int J Oncol. 2011; 38:1245–52. [PubMed: 21369699]
44. Huang W, Dong Z, Wang F, Peng H, Liu JY, Zhang JT. A small molecule compound targeting STAT3 DNA-binding domain inhibits cancer cell proliferation, migration, and invasion. ACS chemical biology. 2014; 9:1188–96. [PubMed: 24661007]
45. Don-Doncow N, Escobar Z, Johansson M, Kjellstrom S, Garcia V, Munoz E, et al. Galiellalactone is a direct inhibitor of the transcription factor STAT3 in prostate cancer cells. J Biol Chem. 2014; 289:15969–78. [PubMed: 24755219]
46. Page BD, Fletcher S, Yue P, Li Z, Zhang X, Sharmeen S, et al. Identification of a non-phosphorylated, cell permeable, small molecule ligand for the Stat3 SH2 domain. Bioorg Med Chem Lett. 2011; 21:5605–9. [PubMed: 21788134]
47. Zhang X, Yue P, Page BD, Li T, Zhao W, Namanja AT, et al. Orally bioavailable small-molecule inhibitor of transcription factor Stat3 regresses human breast and lung cancer xenografts. Proc Natl Acad Sci U S A. 2012; 109:9623–8. [PubMed: 22623533]
48. Eiring AM, Page BD, Kraft IL, Mason CC, Vellore NA, Resetca D, et al. Combined STAT3 and BCR-ABL1 inhibition induces synthetic lethality in therapy-resistant chronic myeloid leukemia. Leukemia. 2015; 29:586–97. [PubMed: 25134459]
49. Haftchenary S, Luchman HA, Jouk AO, Veloso AJ, Page BD, Cheng XR, et al. Potent Targeting of the STAT3 Protein in Brain Cancer Stem Cells: A Promising Route for Treating Glioblastoma. ACS medicinal chemistry letters. 2013; 4:1102–7. [PubMed: 24900612]
50. Page BD, Ball DP, Gunning PT. Signal transducer and activator of transcription 3 inhibitors: a patent review. Expert opinion on therapeutic patents. 2011; 21:65–83. [PubMed: 21114420]
51. Longati P, Jia X, Eimer J, Wagman A, Witt MR, Rehnmark S, et al. 3D pancreatic carcinoma spheroids induce a matrix-rich, chemoresistant phenotype offering a better model for drug testing. BMC Cancer. 2013; 13:95. [PubMed: 23446043]
52. Yamada KM, Cukierman E. Modeling tissue morphogenesis and cancer in 3D. Cell. 2007; 130:601–10. [PubMed: 17719539]
53. Vasko MR, Guo C, Kelley MR. The multifunctional DNA repair/redox enzyme Ape1/Ref-1 promotes survival of neurons after oxidative stress. DNA Repair (Amst). 2005; 4:367–79. [PubMed: 15661660]
54. Sempere LF, Gunn JR, Korc M. A novel 3-dimensional culture system uncovers growth stimulatory actions by TGFbeta in pancreatic cancer cells. Cancer Biol Ther. 2011; 12:198–207. [PubMed: 21613822]
55. Lovborg H, Nygren P, Larsson R. Multiparametric evaluation of apoptosis: effects of standard cytotoxic agents and the cyanoguanidine CHS 828. Mol Cancer Ther. 2004; 3:521–6. [PubMed: 15141009]
56. Lindblom P, Berg AL, Zhang H, Westerberg R, Tugwood J, Lundgren H, et al. Tesaglitazar, a dual PPAR-alpha/gamma agonist, hamster carcinogenicity, investigative animal and clinical studies. Toxicol Pathol. 2012; 40:18–32. [PubMed: 22131108]
57. Nikolovska-Coleska Z, Wang R, Fang X, Pan H, Tomita Y, Li P, et al. Development and optimization of a binding assay for the XIAP BIR3 domain using fluorescence polarization. Anal Biochem. 2004; 332:261–73. [PubMed: 15325294]

58. Friesner RA, Murphy RB, Repasky MP, Frye LL, Greenwood JR, Halgren TA, et al. Extra precision glide: docking and scoring incorporating a model of hydrophobic enclosure for protein-ligand complexes. J Med Chem. 2006; 49:6177–96. [PubMed: 17034125]

59. Halgren TA, Murphy RB, Friesner RA, Beard HS, Frye LL, Pollard WT, et al. Glide: a new approach for rapid, accurate docking and scoring. 2. Enrichment factors in database screening. J Med Chem. 2004; 47:1750–9. [PubMed: 15027866]

60. Luca AC, Mersch S, Deenen R, Schmidt S, Messner I, Schafer KL, et al. Impact of the 3D microenvironment on phenotype, gene expression, and EGFR inhibition of colorectal cancer cell lines. PLoS ONE. 2013; 8:e59689. [PubMed: 23555746]

61. Wilding JL, Bodmer WF. Cancer cell lines for drug discovery and development. Cancer Res. 2014; 74:2377–84. [PubMed: 24717177]

62. Walter K, Omura N, Hong SM, Griffith M, Goggins M. Pancreatic cancer associated fibroblasts display normal allelotypes. Cancer Biol Ther. 2008; 7:882–8. [PubMed: 18344687]

63. Tapia C, Kutzner H, Mentzel T, Savic S, Baumhoer D, Glatz K. Two mitosis-specific antibodies, MPM-2 and phospho-histone H3 (Ser28), allow rapid and precise determination of mitotic activity. Am J Surg Pathol. 2006; 30:83–9. [PubMed: 16330946]

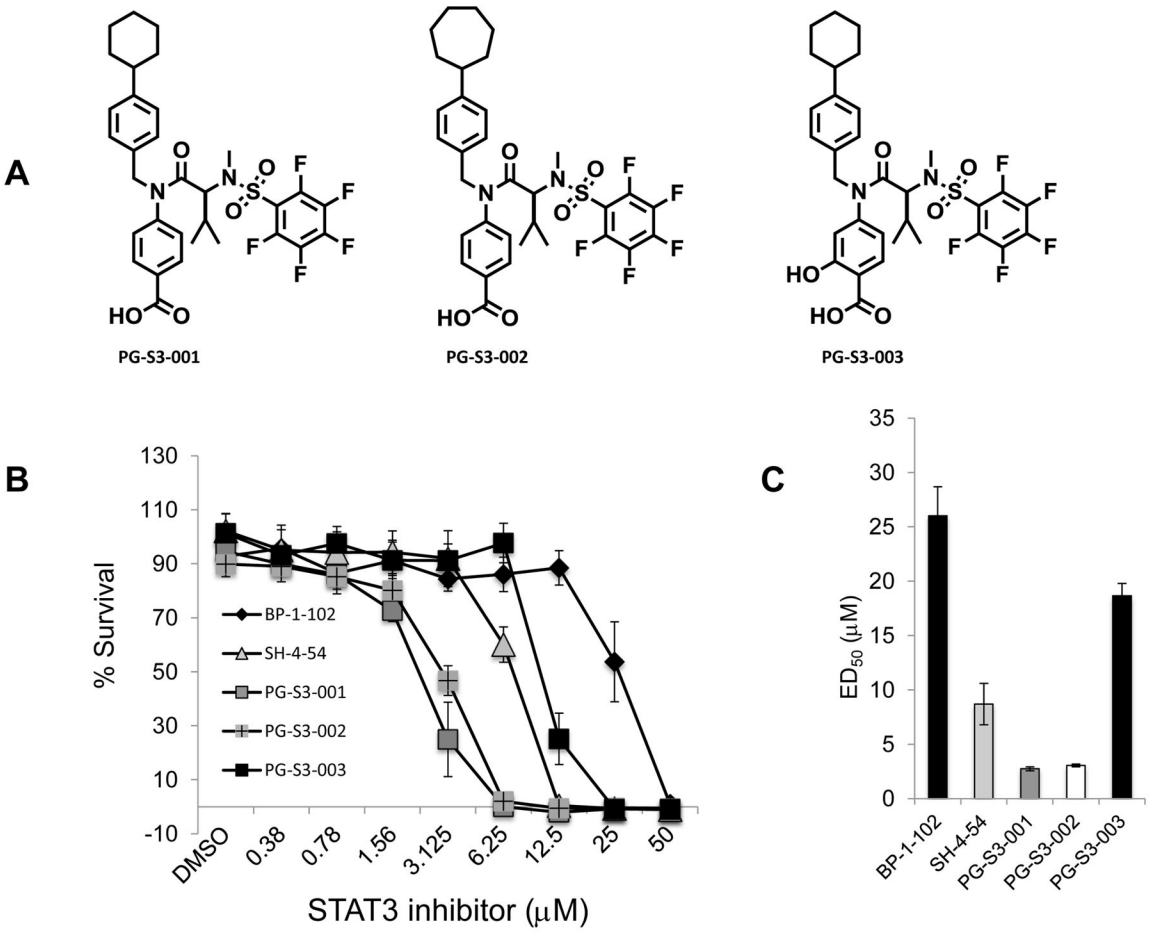

Figure 1.

(A) Structure of lead STAT3 inhibitors: PG-S3-001, PG-S3-002, and PG-S3-003. (B) Top compounds were screened and compared to parent compounds, BP-1-102 and SH4-54, Avg ± SE, n=4–5. (C) Bar graph of ED_{50s} for comparison with new STAT3 inhibitors, Avg±SE, n=4–5.

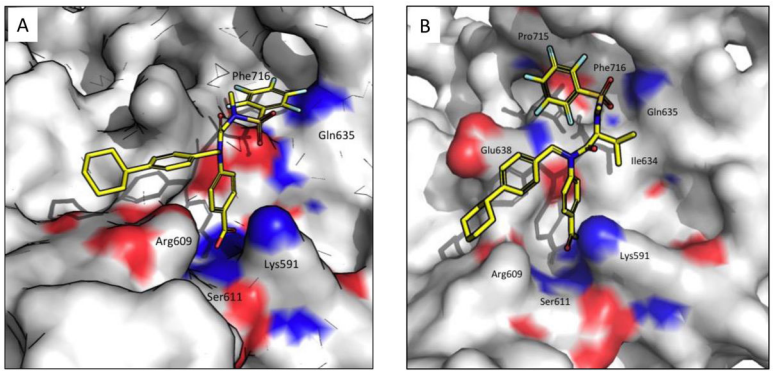

Figure 2.

(A) Computational modeling of PG-S3-001 to the SH2 domain of STAT3: analysis of ligand-receptor interaction. (B) Two-dimensional interaction map highlighting small molecule-receptor interaction of lead compound PG-S3-001.

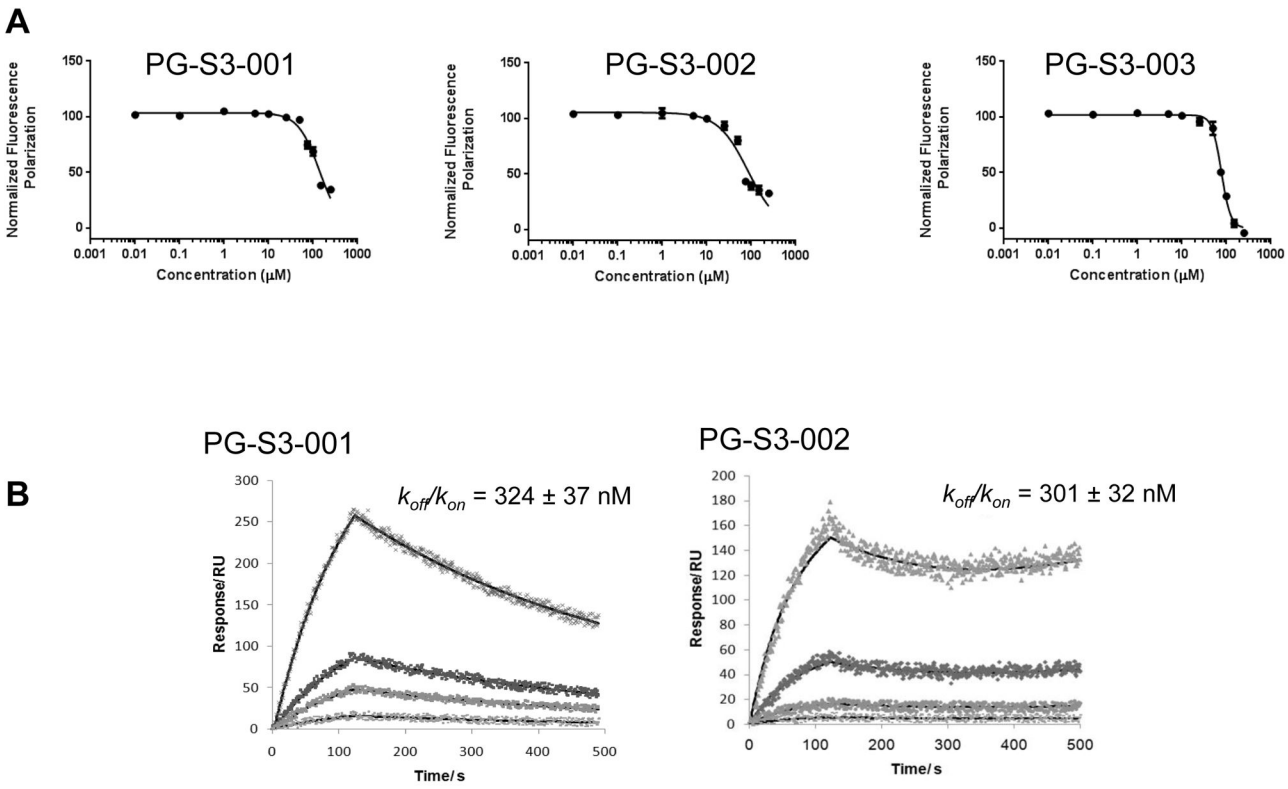

Figure 3.

(A) Fluorescence Polarization (FP) competition assay curves for PG-S3-001, PG-S3-002, PG-S3-003. (B) Surface Plasmon Resonance (SPR) curves displaying the binding affinity for PG-S3-001 and PG-S3-002.

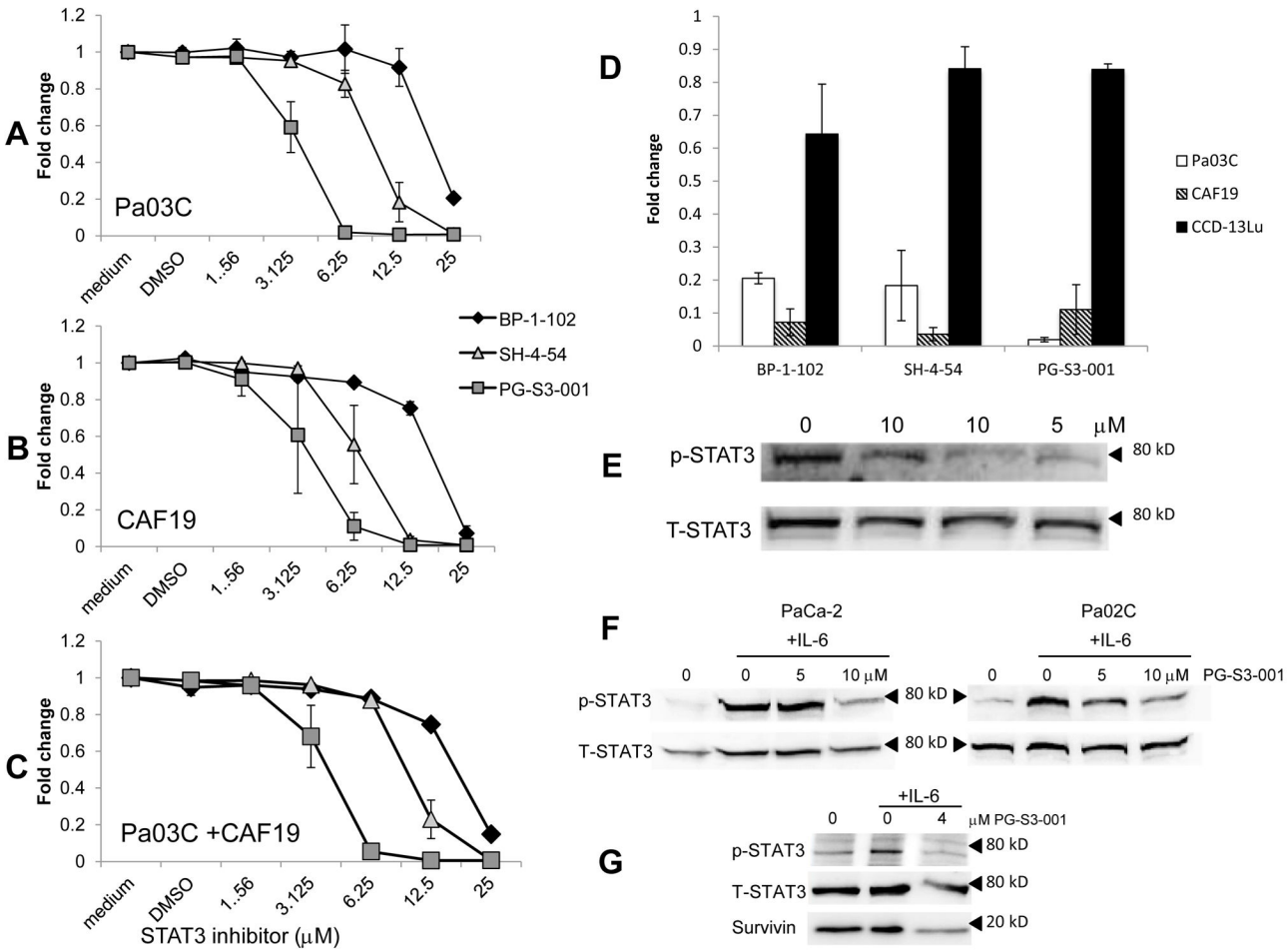

Figure 4.

Lead STAT3 inhibitor, PG-S3-001 effectively disrupts PDAC and CAF cell survival and proliferation individually and in co-culture, but does not affect primary fibroblasts at the doses tested. Dose response curves for lead inhibitor in comparison to parent compounds following 72 hr treatment in low passage patient derived cells, Pa03C (A) CAF19 cells (B) or in the co-culture (2:1 tumor:CAFs, (C) using Alamar blue assay, Avg+SE, n=3–4. (D) Comparison of cytotoxicity in tumor, CAFs, and primary lung fibroblasts of STAT3 inhibitors at the following concentrations: BP-1-102 25μM, SH4-054 12.5μM, and PG-S3-001 6.25μM for 72 hr. Fold change refers to the comparison of each data point to the fluorescence reading of the untreated control. E–G: Immunoblots of whole cells extracts following 4hr pre-treatment with BP-1-102 and SH4-54 (10 μM) and PG-S3-001 (5 μM) in Pa03C cells stimulated with IL-6 (25 ng/mL, 15 min) (E), PDAC cells, PaCa-2 and Pa02C pretreated with increasing amounts of PG-S3-001 for 4 hr and then stimulated with IL-6 ($p<0.05$ for IL-6-treated control vs PG-S3-001 treated cells) (F), and CAF19 cells (G).

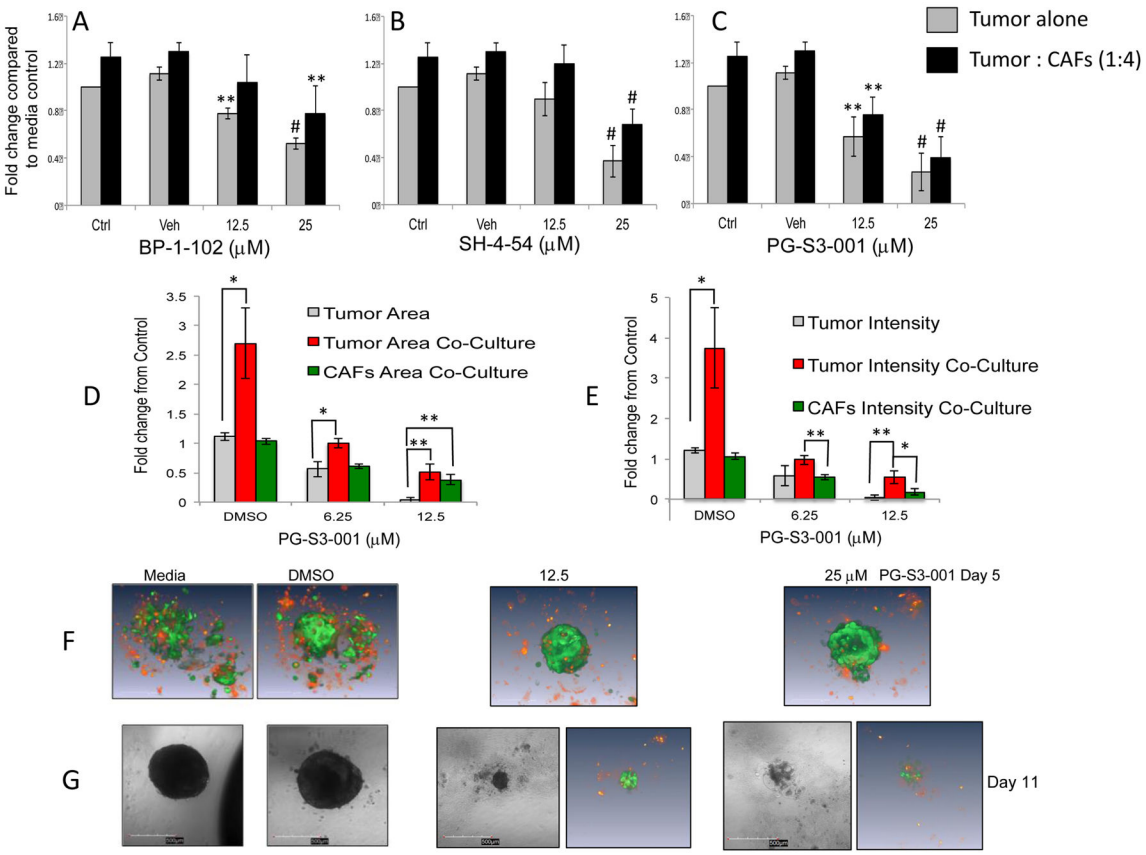

Figure 5.

Inhibition of STAT3 by PG-S3-001 inhibits cell growth in three-dimensional culture systems using proliferation-based assays and confocal microscopy. (A–C) Proliferation assays for lead inhibitor (C) in comparison to parent compounds (A, B) following 12 days in 3D culture. Low passage patient derived spheres, Pa03C (grey bars) or the co-culture spheres (black bars, 1:4 tumor:CAFs) were quantitated using Alamar blue assay, Avg+SE, n=3–4, **p<0.01, #p<0.001 compared to DMSO vehicle control. Quantitation of the images acquired by ArrayScan automated imaging system for the area (D) and the intensity (E) of the red channel and the green channel corresponding to the tumor and the CAFs, respectively. Fold change refers to the comparison of each data point to the fluorescence (RLU) /area of the untreated tumor alone culture. Avg+SE, n=4, * p<0.05, **p<0.01, #p<0.001. 3D reconstruction of images acquired on Day 5 (F) and Day 11 (G) following treatment on Day 3 and 7 of 3D co-cultures with PG-S3-001.

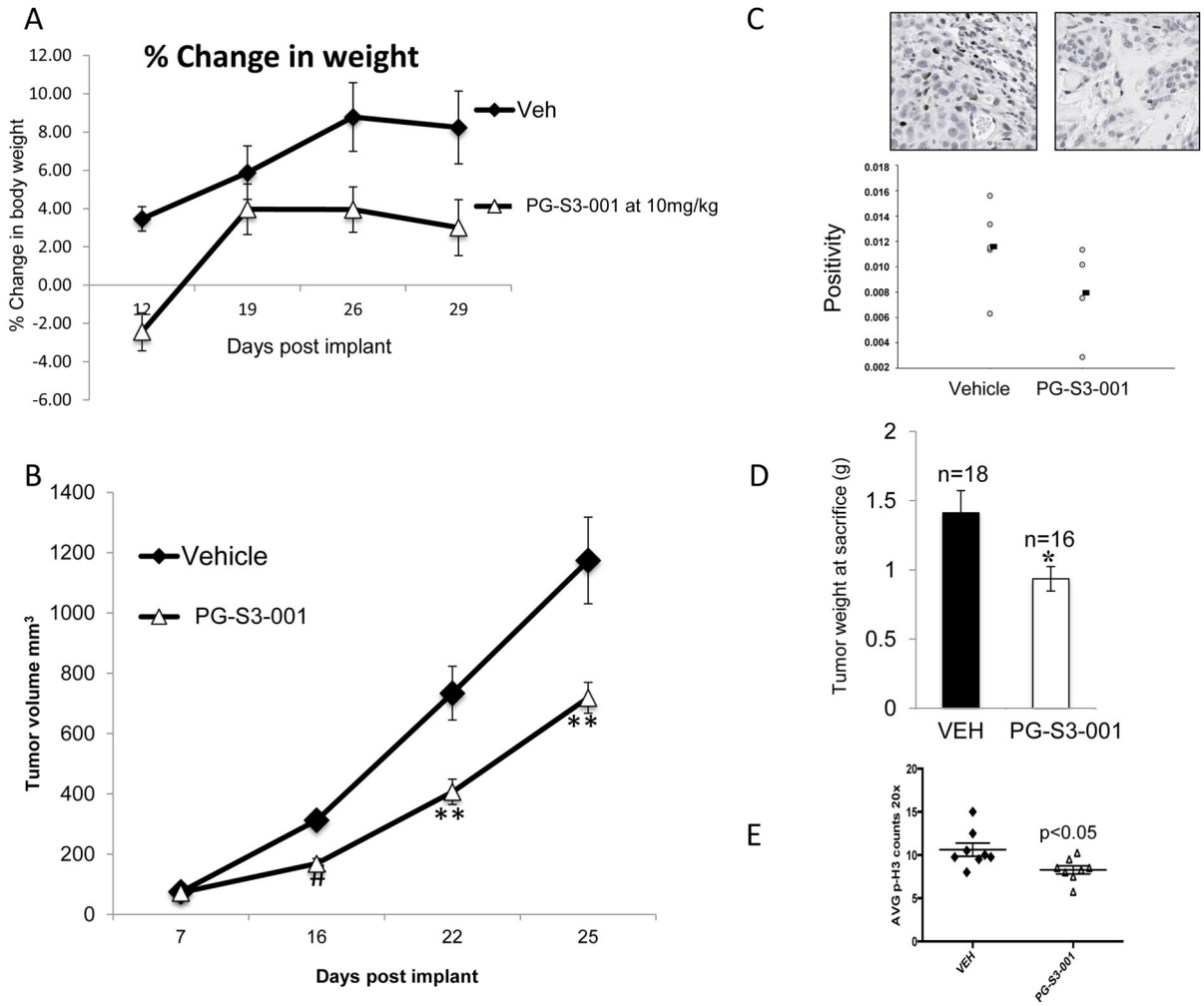

Figure 6.

Significant growth delay on pancreatic cancer xenografts with lead STAT3 inhibitor. NSG mice were implanted with patient-derived cells Pa03C and treated with 10 mg/kg PG-S3-001 for 15 days. There was significant growth delay in the tumors by volume (B) and weight (D) with acceptable body weight loss (A), * $p<0.05$, **$p<0.01$, #$p<0.001$, n=18 for vehicle control treated tumors and n=16 for PG-S3-001. Levels of p-STAT3 (Y705, C) and p-Histone H3 (E, $p<0.05$) were also reduced in the tumors following treatment with STAT3 inhibitor.